Design of Chern and Mott insulators in buckled $3d$-oxide honeycomb bilayers

David Doennig,[1] Santu Baidya,[2] Warren E. Pickett,[3] and Rossitza Pentcheva[2,1,*]

[1] *Forschungs-Neutronenquelle Heinz Maier-Leibnitz (FRM II), Technische Universität München, Lichtenbergstraße 1, 85748 Garching, Germany*

[2] *Department of Physics and Center for Nanointegration Duisburg-Essen (CENIDE), University of Duisburg-Essen, Lotharstr. 1, 47057 Duisburg, Germany*

[3] *Department of Physics, University of California Davis, One Shields Avenue, Davis, CA 95616, U.S.A.*

(Dated: April 2, 2016)

Perovskite $(LaXO_3)_2/(LaAlO_3)_4(111)$ superlattices with X spanning the entire $3d$ transition metal series combine the strongly correlated, multiorbital nature of electrons in transition metal oxides with a honeycomb lattice as a key feature. Based on density functional theory calculations (DFT) including strong interaction effects, we establish trends in the evolution of electronic states as a function of several control parameters: band filling, interaction strength, spin-orbit coupling (SOC) and lattice instabilities. Competition between local pseudocubic and global trigonal symmetry as well as additional flexibility provided by the magnetic and spin degrees of freedom of $3d$ ions, lead to a broad array of distinctive broken symmetry ground states not accessible for the (001)-growth direction, offering a platform to design 2D electronic functionalities. Constraining the symmetry between the two triangular sublattices, X=Mn, Co and Ti emerge as Chern insulators driven by SOC. For X=Mn we illustrate how interaction strength and structure can tune these systems between a Chern and a trivial Mott insulator.

PACS numbers: 73.21.Fg, 73.22.Gk, 75.70.Cn

I. INTRODUCTION

The discovery and investigation of new phases of matter is a major focus of condensed matter physics. Low dimensionality enhances unconventional behavior, and multiorbital active sites introduce additional degrees of freedom, resulting in more complex behavior than can be captured with simple models. Synthesis and characterization of atomically abrupt transition metal oxide (TMO) heterostructures provides such a platform, and several unanticipated functionalities have been discovered, some having the potential to enhance next generation electronics and spintronics devices by controlling charge, spin, orbital, and lattice degrees of freedom at the nanoscale.[1,2]

Topological aspects introduce a new dimension in the search for novel phases. In contrast to the much studied perovskites with (001) growth direction, in the (111) orientation, two triangular BO_6 sublattices of the perovskite ABO_3 structure form a buckled honeycomb lattice, topologically equivalent to graphene. The honeycomb lattice itself introduces exotic possibilities: Haldane obtained a quantum anomalous Hall (QAH) state without explicit external magnetic field,[5]. The model was extended by Wright to a *buckled* honeycomb lattice[6]. Inclusion of SOC[7] and strong interactions[8] provided additional evidence for the robustness of topological states. The lattice models used above are, however, challenging to realize in real materials, and viable Chern insulators remain a much sought goal.

Compared to graphene and common topological insulators (TI), TMOs possess not only larger band gaps, but offer an abundant palette of phases due to several distinctive features: correlated electron behavior causing spin, charge, and orbital instabilities and multi-orbital configurations combined with SOC. The idea of constructing a (111) bilayer from perovskite TMO was introduced by Xiao *et al.* for $4d$ and $5d$ systems, pointing to possibilities for "interface engineering of QAH effects".[9] Building on this foundation, tight-binding models for $(LaNiO_3)_2/LaAlO_3$ demonstrated topological insulating phases can arise from ordering of a complex combination of e_g orbitals.[10,11]

Complementary to tight-binding models, material-specific density functional theory (DFT) can contribute to fundamental understanding as well as guide the search for actual materials realizations. Besides examples for $5d$ systems[12], DFT studies including strong local interaction effects have recently predicted a Dirac-point Fermi surface for $SrTiO_3(111)$[13] and $LaNiO_3(111)$ bilayers,[10,11,14,15] quantum confined within $LaAlO_3$(LAO). In these cases the Dirac point is 'protected' by symmetry; sublattice symmetry breaking leads to a gap-opening due to charge, spin, or orbitally ordered states.[13,15].

To survey the entire band-filling phase diagram and elucidate the underlying *design principles* of functionalities, we have explored systematically the electronic phases in (111)-oriented $(LaXO_3)_2/(LaAlO_3)_4$ superlattices, where X spans the range of trivalent $3d$ ions Ti-Cu. Despite the fact that these systems have nonpolar interfaces we find that unexpected phases including QAH regimes proliferate.

Chern insulators have so far been sought mainly in magnetically doped TIs[16], or by combining trivial magnetic insulators with a material with large SOC, either in double perovskites[17] or rocksalt compounds[18,19]. Of the systems we study, three display simultaneous time re-

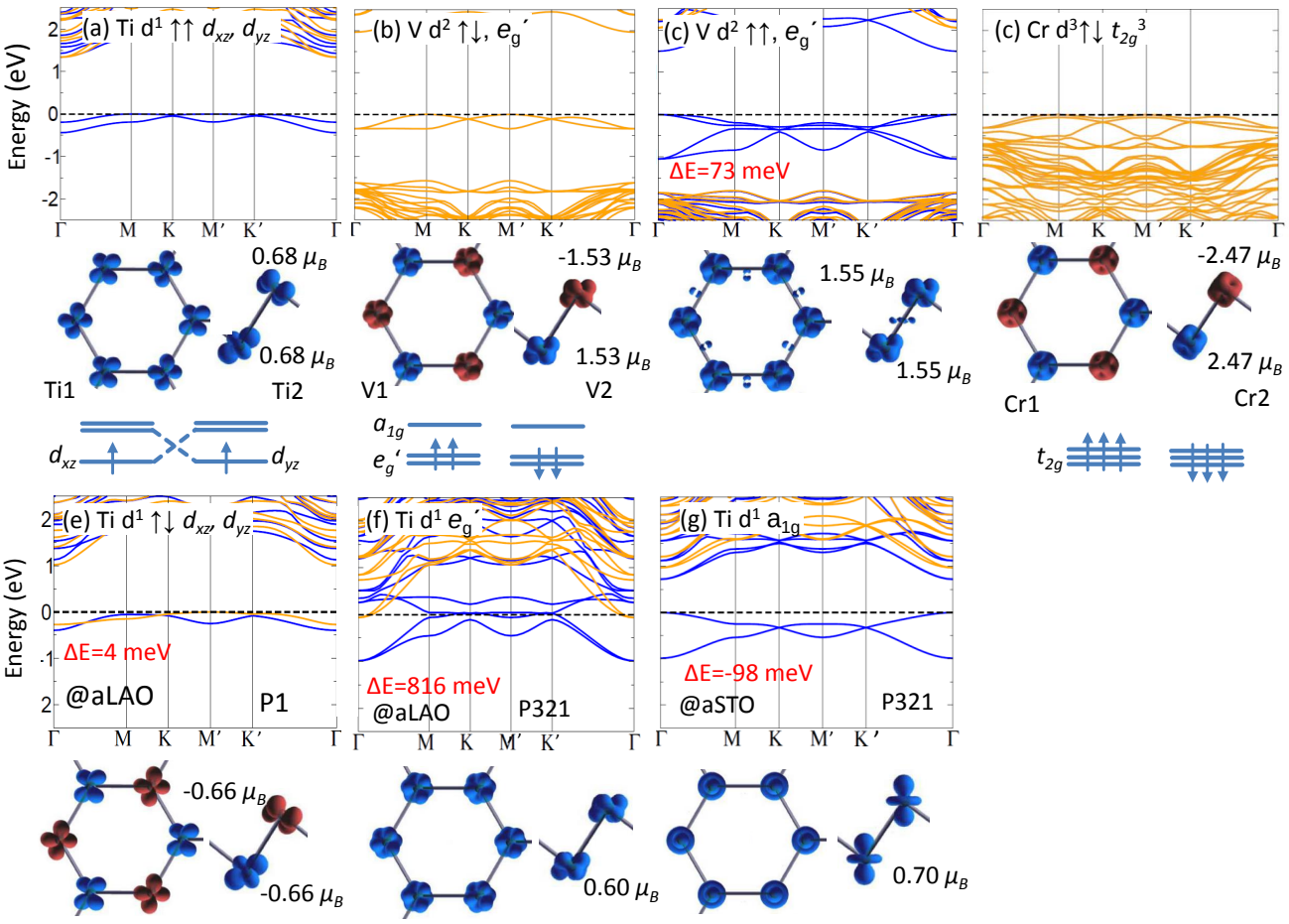

FIG. 1: Electronic ground (a-d) and selected metastable states (c,e-g) in $(LaXO_3)_2/(LaAlO_3)_4(111)$ for t_{2g} systems X=Ti, V, Cr. The majority/minority bands are shown in blue/orange, for the isosurfaces of the spin density majority/minority are in blue/red. In cases (a,e,f,g) the integration range is E_F-1eV,E_F to emphasize the orbital polarization. Energies of metastable states are provided in red.

versal symmetry breaking and SOC-driven gap opening. These examples of Chern insulators in a solely $3d$ system exhibit substantial gap sizes.

II. CALCULATIONAL METHODS

DFT calculations were performed on (111)-oriented $(LaXO_3)_2/(LaAlO_3)_4$ superlattices with $X = 3d$, using the all-electron full-potential linearized augmented-plane-wave (LAPW) method, as implemented in the WIEN2k code[20]. For the exchange-correlation functional we used the generalized gradient approximation (GGA)[21]. Static local electronic correlations were included in the GGA+U approach[22] with U =5 eV, J =0.7 eV (for all X = Ti-Cu $3d$) and U = 8 eV (La $4f$), but the ground states are robust with respect to variation of U in a reasonable range of values. Additional calculations with the modified Becke-Johnson[23] potential support the obtained electronic behavior. The lateral lattice constant is fixed to a_{LAO}=3.79 Å, corresponding to superlattices grown on a LAO(111) substrate, unless otherwise stated, while the out-of-plane lattice parameter c was optimized. Octahedral tilts and distortions were fully taken into account when relaxing atomic positions. SOC was included in several cases using the second-variational method.

III. GROUND AND METASTABLE STATES

A. t_{2g}-systems

A central aspect in the $(LaXO_3)_2/(LaAlO_3)_4(111)$ honeycomb bilayers is their strong deviation from their bulk analogs. Certain recurring features tied to the t_{2g}

and e_g distinction can be identified, thus we discuss them separately. For the t_{2g} subshell the dominating feature is a competition between local pseudo-cubic symmetry and the underlying threefold+inversion symmetry ("P321") of the ideal bilayer: The (111) bilayering reduces the octahedral symmetry to trigonal and splits the t_{2g} orbital triplet into a_{1g} + e'_g. Breaking this symmetry allows occupation of the cubic d_{xy}, d_{yz}, or d_{xz} orbitals.

X=Ti^{3+} $3d^1$. The above scenario arises most vividly for the $LaTiO_3$ bilayer, which displays the richest behavior among the t_{2g} systems. In contrast to bulk $LaTiO_3$ which is a distorted *Pbnm*, G-type antiferromagnetic (AFM) Mott insulator with $1/\sqrt{3}(d_{xy}+d_{yz}+d_{zx})$ orbital order[27,28], the ground state at the lateral lattice constant of $LaAlO_3$ ($a_{\rm LAO}$) (Fig. 1a) is a ferromagnetic (FM) Mott insulator. An unusual staggered d_{xz}, d_{yz} orbital ordering results in a very narrow (0.2 eV bandwidth) lower Hubbard band. This extremely localized character persists also for the AFM state (Fig. 1e) which shows the same orbital polarization and is only 4 meV/u.c. higher in energy, suggesting a weak exchange coupling of ∼1 meV.

An e'_g orbital polarization is achieved by constraining to P321 space group with symmetry-equivalent Ti ions. The degeneracy prevents the opening of a Mott insulating gap and presents a special case of strong correlation effects being rendered ineffectual by an imposed symmetry. Despite its high energy cost of 0.4 eV/Ti, this state is noteworthy due to the unusual direction reversal of bands in the vicinity of K and K′ (Fig. 1f). This intertwining of bands suggests topological character and will be discussed in Sec. IV.

Ti orbital polarization is highly susceptible to strain-tuning: applying tensile strain by imposing the lateral lattice constant of $SrTiO_3$ tips the pseudo-cubic/trigonal symmetry balance and stabilizes occupation of the a_{1g} orbital (Fig. 1g). The band structure just below the gap is comprised of two filled bands with Dirac crossings at K and K′, similar to the LAO/STO(111) case,[15] where the $3d^{0.5}$ band filling fixes the Dirac points at $E_{\rm F}$ instead.

X =V^{3+} $3d^2$. In the $LaVO_3$ bilayer trigonal symmetry splitting dominates over the pseudocubic crystal field: The AFM ground state, displayed in Fig. 1b, is gapped due to occupation of the majority e'_g doublet. This is insensitive to strain and at variance with the bulk G-type d_{xz}, d_{yz} orbital ordering (d_{xy} is occupied on all sites)[28,29]. The FM state (Fig. 1c) with the same orbital polarization is 73 meV/u.c. higher in energy. The set of four bands, topologically similar to those of the metastable $2LaTiO_3$ case (Fig. 1f), is here entirely filled.

X =Cr^{3+} $3d^3$. The Cr bilayer is electronically trivial: a half-filled t_{2g}-band ($t^3_{2g,\uparrow}$, S=$\frac{3}{2}$), thus no orbital degrees of freedom, and antiferromagnetic order (Fig. 1d).

B. e_g-systems

Now we turn to the e_g systems: Consistent with the tight-binding model of Xiao *et al.*[9] a distinctive set of four bands emerges for a FM open e_g subshell: nearly flat bottom and top bands interconnected by two dispersive bands, providing a Dirac point crossing at the K and K′ points and quadratic contact with the flat bands at the Γ point (cf. Fig. 2a-c,h). A key finding is that a pinning of the Dirac point at $E_{\rm F}$ is not solely determined by band filling, but also by an interplay of orbital and spin degrees of freedom, as proven for the cases of X =Mn, Co and Ni. Equivalence of the two sublattices is found to be broken in *all* e_g system ground states where the Dirac point is initially at the Fermi level with distinct origins of symmetry breaking and the resulting gap opening.

X=Mn^{3+} $3d^4$. Within P321 symmetry a Dirac-point Fermi surface results (Fig.2a) from the half-filled $e_{g,\uparrow}$-band of the high-spin Mn ion ($t^3_{2g,\uparrow}e^1_{g,\uparrow}$). Releasing structural symmetry restrictions leads to a Jahn-Teller (JT) distortion with an elongation of the apical Mn-O bond lengths to 2.07-2.11 Å and variation of the basal distances between 1.89-1.98 Å, associated with alternating $d_{3y^2-r^2}$, $d_{3x^2-r^2}$ occupation on the A and B sublattices (Fig. 2e). This symmetry breaking opens a gap of 0.8 eV and also lifts the quadratic band touching degeneracy at Γ. The Jahn-Teller distortion is also present in the AFM order (Fig.2i), which is 88 meV/u.c. higher in energy.

X=Fe^{3+} $3d^5$. The ground state of the $LaFeO_3$ bilayer is a HS AFM band insulator with nearly spherically symmetric charge and spin density on the Fe site, characteristic of a half-filled $3d$ band (S=$\frac{5}{2}$, cf. Fig 2d). For comparison, bulk $LaFeO_3$ is a G-type AFM with orthorhombic *Pnma* structure. The metastable FM configuration (Fig 2l) displays the previously discussed set of four bands, albeit now these are fully occupied for the majority spin channel.

X=Co^{3+} $3d^6$. The $LaCoO_3$ bilayer exhibits an abundant phase diagram with respect to spin degrees of freedom. We note that bulk $LaCoO_3$ has a low spin (LS) (t^6_{2g}) ground state, but becomes ferromagnetic e.g. as a strained film[30]. Constraining symmetry to P321 renders another case where the Fermi level is pinned at the Dirac point (Fig. 2b) with Co being in the intermediate spin (IS) state (t^5_{2g}, e^1_g). Orbital ordering of the e_g electron and t_{2g} hole leads to a FM insulator (0.21 eV lower in energy) with a Co moment of $1.97\mu_B$ (Fig. 2f). A further metastable state, only 19 meV less favorable, exhibits a new type of *spin state symmetry breaking* where the two Co sublattices assume IS and LS states with very flat bands accompanied by a $d_{x^2-y^2}$ orbital occupation on the IS Co sublattice (Fig.2j).

X=Ni^{3+} $3d^7$. While bulk $LaNiO_3$ is a $R\bar{3}c$ correlated metal[27], a Dirac-point Fermi surface is obtained for the $LaNiO_3$ bilayer[10,11,15] within P321 symmetry (cf. Fig. 2c). Relaxation induces disproportionation at the Ni sites, expressed in different magnetic moments of 1.30 and 1.08 $\mu_{\rm B}$, and opens a gap of 0.25 eV at the Fermi level (cf. Fig. 2g)[15]. AFM coupling of the two bilayers results in flat bands (Fig.2j), defining a band gap of ∼ 1 eV with orbital polarization at the Ni sites, as recently observed in a $NdNiO_3$ bilayer.[31] This illustrates how an-

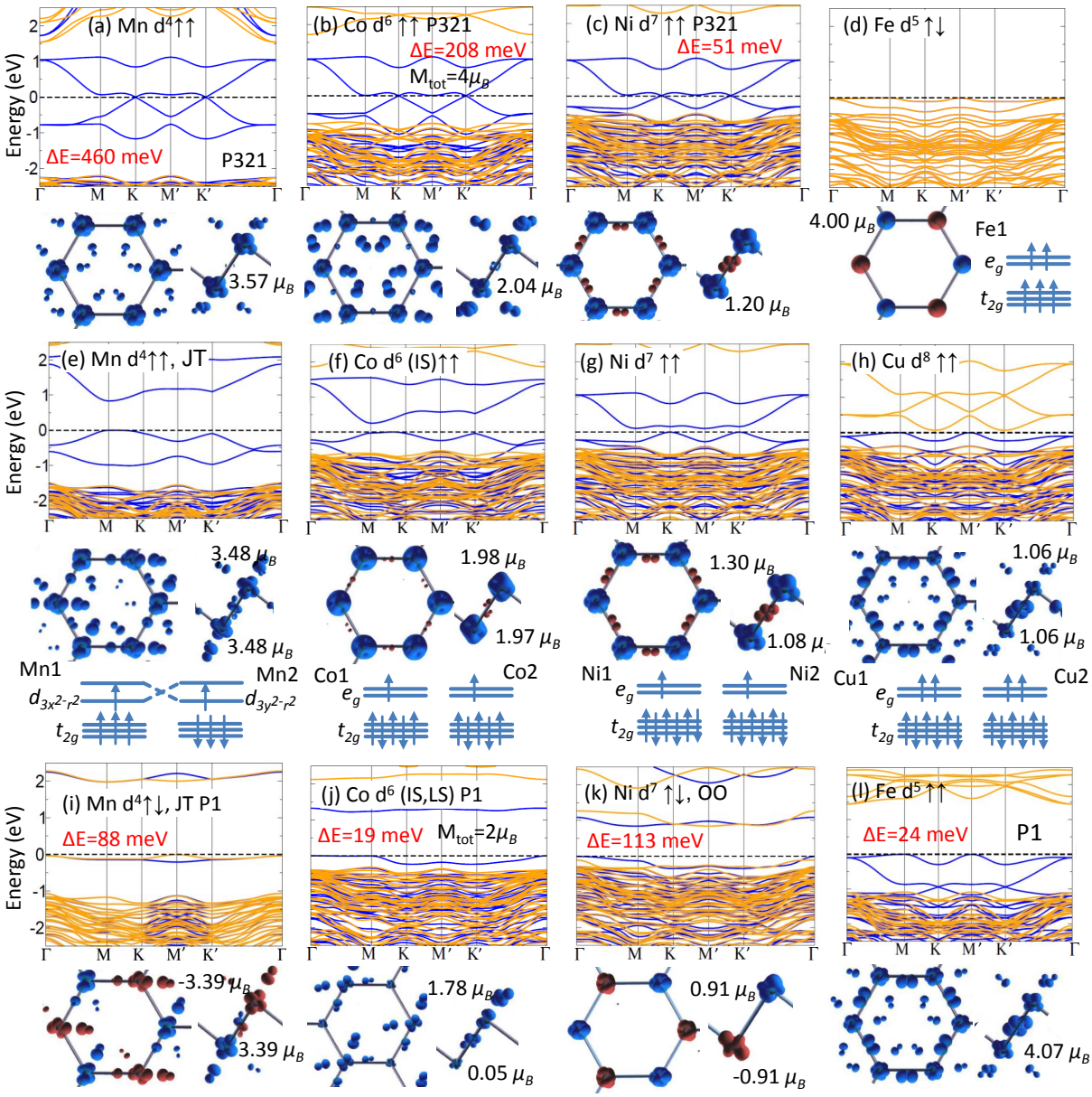

FIG. 2: Presentation as in Fig. 1, but for e_g systems X=Mn, Fe, Co, Ni, and Cu. A common feature is a set of four bands - two nearly flat and two crossing at K and K′. Despite the formally different band filling in X=Mn, Co, Ni a Dirac point Fermi surface arises within P321 (a)-(c), while symmetry breaking results in a gap opening d(e)-(g). Further metastable phases are shown in Fig. (i)-(l).

tiferromagnetic order provides the necessary decoupling of the two trigonal bilayers, analogous to the La_2NiAlO_6 double perovskite where the single triangular Ni-layers are separated by Al-layers[15].

X=Cu^{3+} $3d^8$ yields an $e_{g,\uparrow}^2$ S=1 ion at half filling of the e_g bands, where the occupied (majority) and unoccupied (minority) set of four bands are separated by a very low energy spin-flip excitation gap (Fig. 2h, see also[9]). Although Cu^{3+} is uncommon (bulk $LaCuO_3$ is metallic and must be synthesized under pressure),[32] it might be stabilized by non-equilibrium epitaxial synthesis.

IV. SPIN-ORBIT COUPLING AND TOPOLOGICAL CHARACTER

Spin-orbit coupling, recognized as important in $4d$ and especially $5d$ materials, displays an unexpectedly strong effect for X =Ti, Mn, and Co bilayers. Thereby, the symmetry between the two sublattices is crucial. For the Ti bilayer with e_g' orbital polarization SOC with out-of-plane magnetization leads to a band inversion and gap-opening (Fig.3 a). A disparity between K and K′ signals the loss of equivalence of the two Ti ions, reflected

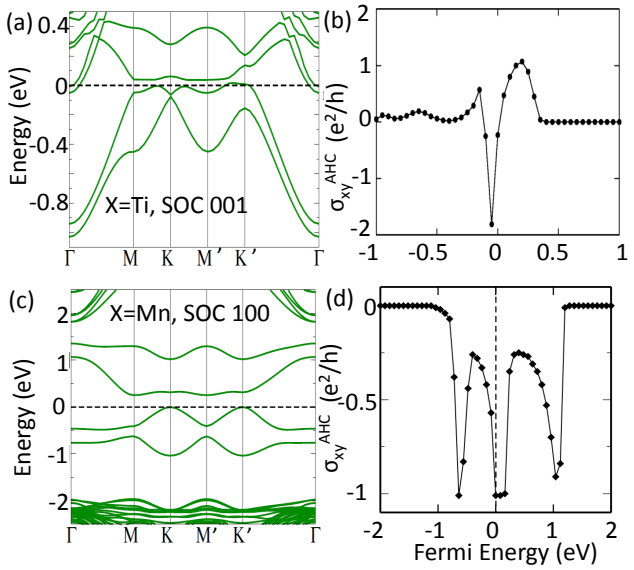

FIG. 3: Effect of SOC on $(LaXO_3)_2/(LaAlO_3)_4$ within P321 symmetry: (a) band inversion and gap opening for X=Ti with out-of-plane magnetization; (c) for X=Mn SOC with magnetization along [100] opens a substantial gap of 0.2 eV and lifts the degeneracy at Γ; (b) and (d) calculated AHC versus (rigid band) chemical potential in units of (e^2/h) indicates quantization of AHC in both cases. Small deviations from the integer value for $X = Ti$ are likely due to other trivial pockets around the Fermi level.

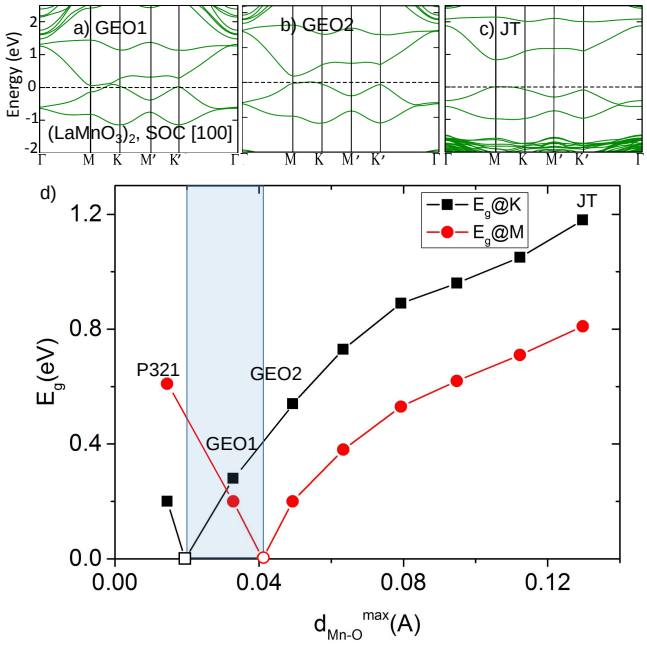

FIG. 4: Transition between the Chern insulating phase within P321 symmetry and the Mott insulating ground state in $(LaXO_3)_2/(LaAlO_3)_4(111)$: The band structures (a-c) show that a crossover of the gap sizes at K and M occurs already for the first geometry along the path (GEO1) which is metallic with a crossing along K-M. d) evolution of band gap at K and M as a function of JT distortion expressed in maximum deviation of Mn-O distance from the average distance in the MnO_6 octahedron. The shaded area denotes the expected metallic region.

in an unexpectedly large orbital moment on only one of the ions: $0.11\mu_B$ versus just $0.01\mu_B$ on the other. Calculation of the anomalous Hall conductivity (AHC)[24–26] indicates integer Chern values (Fig.3 b).

Without SOC, $P321$ symmetry protects the Dirac-point degeneracy of the Mn-bilayer (Fig. 2a). SOC with in-plane magnetization preserves the symmetry connecting the Mn sites (and K, K′ equivalence) but gaps the Dirac-point as well as the quadratic band touching at Γ (Fig.3 c). The calculated AHC,[24–26] in Fig. 3 d, reveals $(LaMnO_3)_2$ with P321 symmetry to be a C=-1 Chern insulator with an impressive gap size of ∼200 meV. Analysis of the effect of Hubbard U shows that the SOC-induced gap opening is interaction-driven and appears beyond a critical strength $U = 3$ eV and $J = 0.7$ eV (For more details see Appendix B). Such an interaction driven enhancement of SOC was recently proposed in Ir-based pyrochlore oxides[33].

As the ground state of the Mn bilayer is a trivial Mott insulator, we have explored the topological transition from the Chern to the trivial Mott insulator by studying several geometries along the distortion path. Fig. 4d displays the evolution of band gaps at the K and M points as the JT distortion of the MnO_6 octahedron proceeds. The gap closing at K and the topological transition occurs for a small but nonzero distortion. The band structure for the first chosen geometry, shown in Fig. 4a, displays overlapping bands between K and M, due to inversion of eigenvalues at K. The bands are disentangled and the Chern number is already quenched. The distortion is accompanied by a crossover of the minimum gap from K (for P321, Chern insulator) to M point (trivial JT phase). In the subsequent geometries along the path the gaps increase monotonically: the gap closing has enabled band disentanglement, after which relaxation and gap opening proceeds rapidly.

In order to maintain the Chern insulating phase, either the SOC strength must be increased or the Jahn-Teller distortion amplitude decreased. Both directions suggest replacement of the $3d$ ion with a $4d$ or $5d$ ion, or alternatively, the exploration of strain, applied bias, or substituting the band insulator $LaAlO_3$ by another material as perspectives for further research.

The control of matter away from equilibrium including access to metastable states is one of the current grand challenges in condensed matter science[34]. An appealing path to achieve the metastable QAHI state may involve selective excitation of phonon modes, as recently demonstrated for (001) nickelate superlattices where a metal-to-insulator transition is induced through femtosecond midinfrared radiation[35].

V. SUMMARY

Our mapping of the variety of states across the 3*d* series of perovskite-derived oxide honeycomb lattices reveals the prominent role of band filling, SOC strength, structural distortion (orbital ordering), and interaction strength, evidently with complex interplay between them. Conservation of the symmetry between the two sublattices is crucial and enables Chern insulator phases with gaps up to a few hundred meV, large enough to enable room temperature study and applications if this state can be stabilized (several paths towards the realization were outlined above). Even beyond the topological aspects, the phase diagram exhibits a variety of unanticipated ground states, arising from assorted symmetry-breaking forces and leading to orbital and charge states that are not accessible in the bulk or (001) oriented superlattices. The simultaneous time-reversal and inversion symmetry breaking implies multiferroic behavior, a finite dipole seems likely in particular in cases of disproportionation of the two sublattices as e.g. in $LaNiO_3$ or the polar $(STO)_2/LAO(111)$[13] system. Thus the $LaXO_3(111)$ bilayers with $X = 3d$ represent a rich playground to tailor 2D functionality in oxide materials.

APPENDIX A: INFLUENCE OF SPIN ORBIT COUPLING ON THE ELECTRONIC PROPERTIES OF $(LaCoO_3)_2/(LaAlO_3)_4$(111) SLS

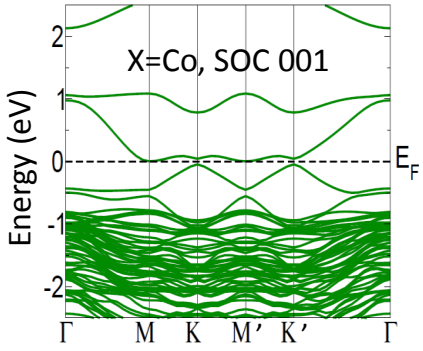

FIG. 5: Influence of SOC with magnetization axis along [001] on the band structure of $(LaCoO_3)_2(LaAlO_3)_4$(111) (P321). Note the gap opening at K and the lifting of degeneracy at Γ.

In Fig.5 we show the effect of SOC with magnetization along the [001] directon on the band structure of the $LaCoO_3$ bilayer. As for $LaMnO_3$ (Fig.3 c), SOC gaps the band structure at K and K′ and the quadratic band touching point at Γ, but overall the effect is smaller than for the LMO bilayer. Recently, also $LaCoO_3$(111) sandwiched within $SrTiO_3$ was reported to be a Chern insulator[36]: in this system the polar discontinuity at the interface results in a different band filling where only the bottom flat band is occupied and the Fermi level is at the quadratic band touching point prior to SOC.

APPENDIX B: INFLUENCE OF THE ON-SITE COULOMB REPULSION PARAMETER U ON THE ELECTRONIC PROPERTIES OF $(LaMnO_3)_2/(LaAlO_3)_4$(111) SLS

In the following we investigate the influence of U on the band structure and anomalous Hall conductivity for the high symmetry phase P321 of $(LaXO_3)_2/(LaAlO_3)_4$(111). The band structures calculated within GGA+U+SOC with magnetization axis along the [100] crystallographic direction for U=2-5eV and J=0.7 eV and the corresponding anomalous Hall conductivity are presented in Fig. 6.

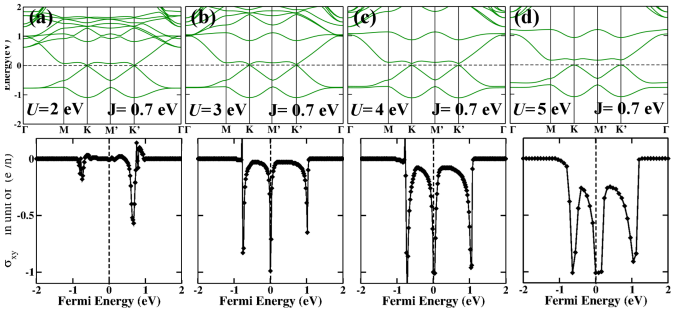

FIG. 6: Band structure (top row) and corresponding anomalous Hall conductivity in units of quantum conductance (e^2/h) (bottom row) of $(LaMnO_3)_2/(LaAlO_3)_4$ (P321) as a function of Hubbard U in P321 symmetry. Note that the band gap at K opens above $U = 3$ eV, $J = 0.7$ eV

We find that for smaller values, e.g. $U = 2$ eV, $J = 0.7$ eV the gap at K is closed but opens and increases gradually with increasing U. Concerning the anomalous Hall conductivity: For $U = 2$ eV AHC is finite but smaller than one. The main features of the Chern insulating state with an integer value of $C = -1$ for the lower band emerge for $U = 3$ and beyond. This emphasizes that the Chern insulating state is interaction-driven: Only the combination of spin-orbit coupling and strong Coulomb repulsion is able to open a gap at K and K′ points. We note that a U value of 4.5 eV was obtained for bulk $LaMnO_3$[37] using the linear response approach of Cococcioni and Gironcoli[38], which is very close to the value we have used for the $LaMnO_3$ bilayer (U=5.0 eV and $J = 0.7$ eV) and justifies our choice. Determination of the U values for the 3*d* oxide bilayers would be an useful aspect of future studies.

Since submission of this paper we became aware of work by Weng et a.[39] on $(LaMnO_3)_2/LaScO_3$(111), that shows overall a similar behavior.

ACKNOWLEDGMENTS

Discussions with Binghai Yan are gratefully acknowledged. This work was partially supported by the German Science Foundation within SFB/TR80, project G3 (to R.P.) and by U.S. Department of Energy Grant No. DE-FG02-04ER46111 (to W.E.P.).

* Electronic address: Rossitza.Pentcheva@uni-due.de

[1] H. Y. Hwang, Y. Iwasa, M. Kawasaki, B. Keimer, N. Nagaosa and Y. Tokura, Nat. Mater. **11**, 103 (2012).
[2] J. Mannhart, and D. G. Schlom, Science **327**, 1607 (2010).
[3] S. Middey, D. Meyers, M. Kareev, E. J. Moon, B. A. Gray, X. Liu, J. W. Freeland and J. Chakhalian, Appl. Phys. Lett. **101**, 261602 (2012).
[4] M. Gibert, P. Zubko, R. Scherwitzl and J.-M. Triscone, Nat. Mater. **11**, 195 (2012).
[5] F. D. M. Haldane, Phys. Rev. Lett. **61**, 2015 (1988).
[6] A. R. Wright, Sci. Rep. **3**, 2736 (2013).
[7] C. L. Kane and E.J. Mele, Phys. Rev. Lett. **95**, 226801 (2005).
[8] S. Raghu, X. L. Qi, C. Honerkamp and S.-C. Zhang, Phys. Rev. Lett. **100**, 156401 (2008).
[9] D. Xiao, W. Zhu, Y. Ran, N. Nagaosa and S. Okamoto, Nature Commun. **2**, 596 (2011).
[10] K.-Y. Yang, W. Zhu, D. Xiao, S. Okamoto, Z. Wang and Y. Ran, Phys. Rev. B **84**, 201104(R) (2011).
[11] A. Rüegg and G. A. Fiete, Phys. Rev. B **84**, 201103 (2011).
[12] J. L. Lado, V. Pardo and D. Baldomir, Phys. Rev. B **88**, 155119 (2013).
[13] D. Doennig, W. E. Pickett and R. Pentcheva, Phys. Rev. Lett. **111**, 126804 (2013).
[14] A. Rüegg, C. Mitra, A.A. Demkov and G. A. Fiete, Phys. Rev. B **85**, 245131 (2012); ibid. **88** 115146 (2013).
[15] D. Doennig, W. E. Pickett and R. Pentcheva, Phys. Rev. B **89**, 121110 (2014).
[16] C.-Z. Chang, *et al.*, Science **340**, 167 (2013).
[17] A. M. Cook, A. Paramekanti, Phys. Rev. Lett. **113**, 077203 (2014).
[18] K. F. Garrity and D. Vanderbilt, Phys. Rev. B **90**, 121103(R) (2014).
[19] H. Zhang, J. Wang, G. Xu, Y. Xu and S.-C. Zhang, Phys. Rev. Lett. **112**, 096804 (2014).
[20] P. Blaha, K. Schwarz, G. K. H. Madsen, D. Kvasnicka, and J. Luitz, *WIEN2k, An Augmented Plane Wave Plus Local Orbitals Program for Calculating Crystal Properties*, ISBN 3-9501031-1-2 (Vienna University of Technology, Vienna, Austria, 2001).
[21] J. P. Perdew, K. Burke and M. Ernzerhof, Phys. Rev. Lett. **77**, 3865 (1996).
[22] V. I. Anisimov, J. Zaanen and O. K. Andersen, Phys. Rev. B **44**, 943 (1991).
[23] F. Tran and P. Blaha, Phys. Rev. Lett. **102**, 226401 2009.
[24] A. A. Mostofi, J. R. Yates, Y. S. Lee, I. Souza, I. Vanderbilt and N. Marzari, Comput. Phys. Commun. **178**, 685 (2008).
[25] X. Wang, J. R. Yates, I. Souza and D. Vanderbilt, Phys. Rev. B **74**, 195118 (2006).
[26] J. Kuneš, R. Arita, P. Wissgott, A. Toschi, H. Ikeda and K. Held, Comp. Phys. Commun. **181**, 1888 (2010).
[27] T. Arima, Y. Tokura and J. B. Torrance, Phys. Rev. B **48**, 17006 (1993).
[28] E. Pavarini, S. Biermann, A. Poteryaev, A. I. Lichtenstein, A. Georges and O. K. Andersen, Phys. Rev. Lett. **92**, 176403 (2004).
[29] M. De Raychaudhury, E. Pavarini, O.K. Andersen, Phys. Rev. Lett. **99**,126402 (2007).
[30] H. Hsu, P. Blaha and R. M. Wentzcovitch, Phys. Rev. B **85**, 140404 (2012).
[31] S. Middey, D. Meyers, D. Doennig, M. Kareev, X. Liu, Y. Cao, Zhenzhong Yang, Jinan Shi, Lin Gu, P. J. Ryan, R. Pentcheva, J.W. Freeland and J. Chakhalian, Phys. Rev. Lett. **116**, 056801 (2016).
[32] M. Karppinen, H. Yamauchi, T. Ito, H. Suematsu and O. Fukunaga, Matl. Sci. & Eng. **41**, 59 (1996).
[33] D. Pesin and L. Balents, Nat. Phys.**6**, 376 (2010).
[34] G. R. Flemming and M.A. Ratner, Phys. Today **61**, 28 (2008).
[35] A. D. Caviglia, R. Scherwitzl, P. Popovich, W. Hu, H. Bromberger, R. Singla, M. Mitrano, M. C. Hoffmann, S. Kaiser, P. Zubko, S. Gariglio, J.-M. Triscone, M. Först and A. Cavalleri Phys. Rev. Lett. **108**, 136801 (2012).
[36] Y. Wang, Z. Wang, Z. Fang and X. Dai, Phys. Rev. B **91**, 125139 (2015).
[37] G. Trimarchi and N. Binggeli, Phys. Rev. B **71**, 035101 (2005).
[38] M. Cococcioni and S. de Gironcoli, Phys. Rev. B **71**, 035105 (2005).
[39] Y. Weng, X. Huang, Y. Yao and S. Dong, Phys. Rev. B 92, 195114 (2015).